Supplemental Materials

N-terminal splicing extensions of the human *MYO1C* gene fine-tune the kinetics of the three full-length myosin IC isoforms

Lilach Zattelman[1], Ronit Regev[1], Marko Ušaj[1], Patrick Y. A. Reinke[3], Sven Giese[3], Abraham O. Samson[2], Manuel H. Taft[3], Dietmar J. Manstein[3] and Arnon Henn[1]*

From the Faculty of Biology, Technion- Israel Institute of Technology, Haifa, 3200003, Israel[1], Faculty of Medicine in the Galilee, Bar-Ilan University, Safed 1311520, Israel [2], Institute for Biophysical Chemistry, Hannover Medical School, OE 4350, Carl-Neuberg-Str. 1, 30625 Hannover, Germany[3]

*To whom correspondence should be addressed: Arnon Henn, Faculty of Biology, Technion- Israel Institute of Technology, Haifa, 3200003, Israel. Tel. +947 (4) 8294839; Fax. +947 (4) 8295424; E-mail: arnon.henn@technion.ac.il

Analysis of equilibrium binding of MYO1C and MYO1C·ADP isoforms to pyrene·actin-

Pyrene-labeled actin is linearly quenched by myosin binding, allowing measurement of the binding affinities of MYO1C isoforms to actin in the presence or absence of ADP (1) (Scheme S1, Equation S1).

$$A^{*} + M \underset{}{\overset{K'_{D}}{\rightleftharpoons}} AM$$

$$A^{*} + M \cdot ADP \underset{}{\overset{K'_{DA}}{\rightleftharpoons}} AM \cdot ADP$$

(Scheme S1)

$$\frac{\Delta F}{F_0} = \frac{F_0 - F}{F_0} = \frac{\Delta F_{max}[\text{MYO1C}]}{K'_{A} + [\text{MYO1C}]}$$

(Eq. S1)

Equilibrium binding titration of MYO1C isoforms to pyrene-labeled actin quenched pyrene fluorescence by ~25%, 43%, and 65% for MYO1C^{35}, MYO1C^{16}, and MYO1^{C}, respectively, in the absence or presence of ADP (Figure S4). Actin quenching showed a hyperbolic dependence on myosin concentration, yielding the equilibrium binding constants K'_{DA} and K'_{A} for myosin binding to actin with and without ADP, respectively (Eq. S1, Table S3). The binding affinities of MYO1C^{35} for actin in the absence or presence of ADP ($K'_{A}{}^{35}$ = 9.8 ± 2.4 nM, $K'_{DA}{}^{35}$ = 12.3 ± 1.3 nM) were significantly tighter (> 5-fold) than that of for MYO1C^{16} ($K'_{A}{}^{16}$ = 65.8 ± 20.5 nM, $K'_{DA}{}^{16}$ = 68.3 ± 36.2 nM). The affinity of MYO1C^{C} for actin was decreased further, by 1.1- and 1.2-fold, relative to that of MYO1C^{16} in the absence or presence of ADP ($K'_{A}{}^{C}$ = 72.6 ± 17.9 nM and $K'_{DA}{}^{C}$ = 83.1 ± 29.4 nM).

Figure S1

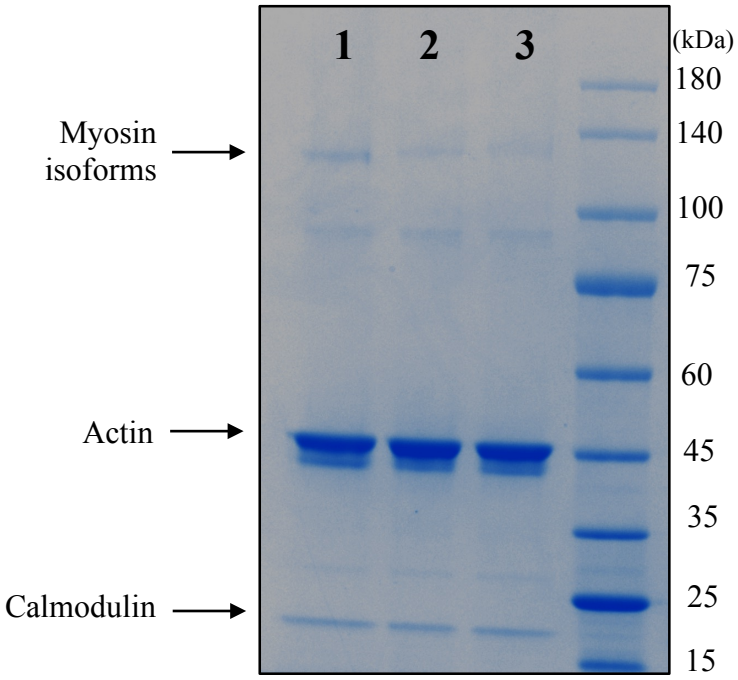

Figure S1. Light-chain calmodulin occupancy of MYO1C isoforms.
Representative SDS-PAGE gels stained with Coomassie Blue for determination of the calmodulin occupancy of the MYO1C isoforms, MYO1C^{C} (lane 1, MW 117.9 kDa), MYO1C^{16} (lane 2, MW 119.2 kDa), and MYO1C^{35} (lane 3, MW 121.7 kDa), as determined by the co-sedimentation assay. The associated calmodulin light chain can be seen in all lanes (~17 kDa). We noticed a minor contaminating band after ultra-centrifugation (~90 kDa), which was most likely a degradation product of myosin. However, calmodulin quantification was performed independently of these additional bands, and the total protein concentration of each isoform was determined independently here as well as in Figure 1C, confirming the high-quality purification of Myo1C isoforms

Figure S2

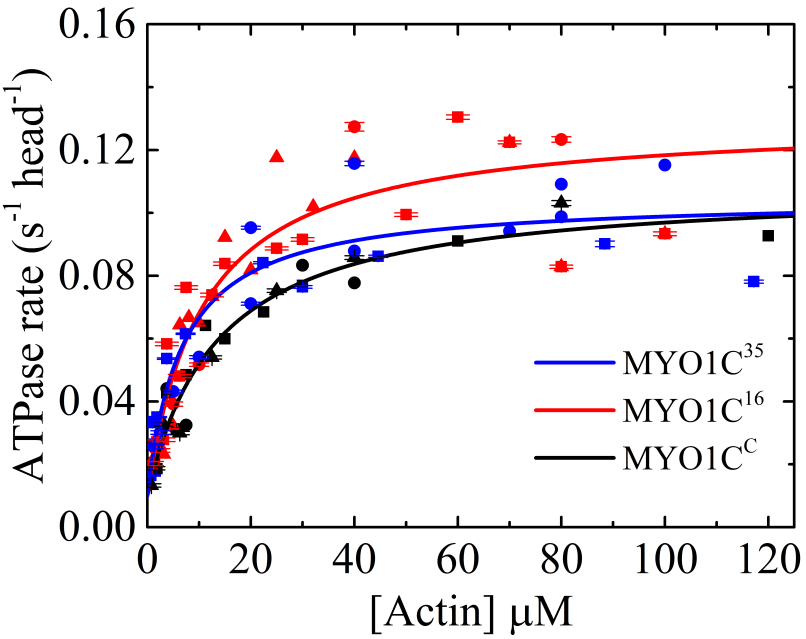

Figure S2. Steady-state ATPase activity of human MYO1C isoforms.
[Actin]-dependence steady-state ATPase activity of 100 nM MYO1C isoforms: MYO1C^{35} (blue), MYO1C^{16} (red), and MYO1C^{C} (black). Solid lines represent the best fit to $= V_0 + \frac{k_{cat}[actin]}{K_{m,ATPase}+[actin]}$. Error bars of the fit are within data points. Data represents measurements conducted with three different protein purifications per construct (■,●,▲). The maximum rates of ATPase activity, k_{cat}, are practically the same for all three isoforms (k_{cat} = 0.09 ± 0.01, 0.12 ± 0.01, 0.09 ± 0.00 s^{-1}·head^{-1}, for MYO1C^{35}, MYO1C^{16}, and MYO1^{C}, respectively). The K_{ATPase} of MYO1C^{C} (13.5 ± 2.00 µM) is 2- and 1.3-fold weaker than those of MYO1C^{35} and MYO1C^{16}, respectively, (6.7 ± 1.57 and 10.6 ± 1.98 µM), which do exhibit some degree of change, but not to the extent of eradicating the actin-dependent behavior of the isoforms.

Figure S3

A.

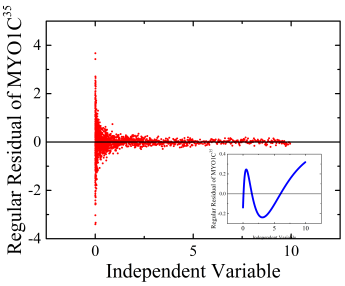

B.

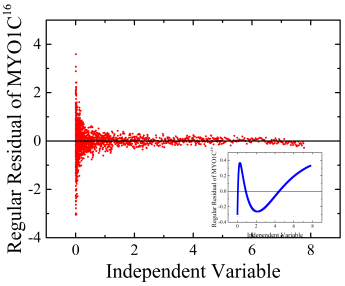

C.

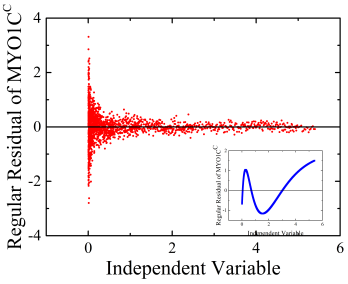

Figure S3. Regular residual analysis of ADP dissociation determined by ATP-induced dissociation of (pyrene)acto·MYO1C.
Representative regular residuals analysis of the representative time courses fitted to the double-exponential function presented in Figure 4A. **A**. MYO1C^{35} **B**. MYO1C^{16} **C**. MYO1C^{C}. The transients obtained after rapid mixing of 2 mM MgATP with an equilibrated mixture of 25 nM pyrene-labeled acto-MYO1C isoforms with 7.5 μM ADP. Insets are the representative regular residuals analysis of the same representative time courses, fitted to a single-exponential function.

Figure S4

A.

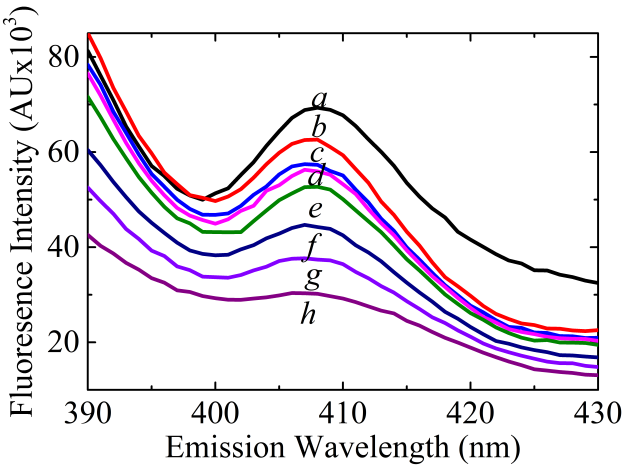

B.

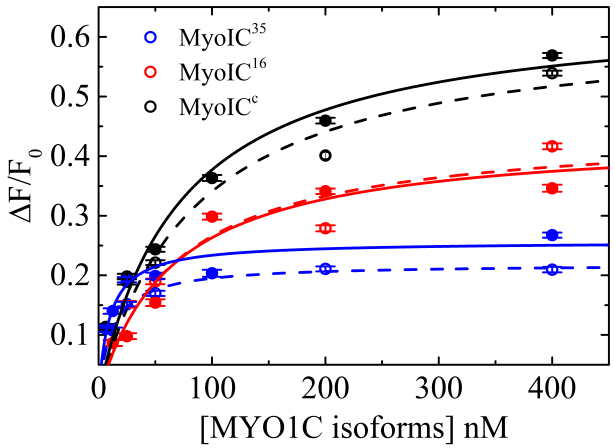

Figure S4. Steady-state measurements of (pyrene)acto·MYO1C binding affinities

A. Representative emission spectrum of 25 nM pyrene·actin fluorescence quenching due to binding of 0 (curve a), 6.25 (curve b), 12.5 (curve c), 25 (curve d), 50 (curve e), 100 (curve f), 200 (curve g), or 400 (curve h) nM MYO1C^{C}. **B**. [MYO1C isoforms]-dependent fractional quenching of pyrene fluorescence, F_0-F/F_0, where F_0 and F are the fluorescence at 409 nm in the absence and presence of myosin, respectively. Standard errors are within data points. MYO1C^{35} (blue), MYO1C^{16} (red), and MYO1C^{C} (black) were analyzed in the absence of ADP (solid circles) and in the presence of 1 mM MgADP (open circles). The solid and dashed lines through the data represent the best fit to Eq. S1 in the absence and presence of ADP, respectively.

igure S5

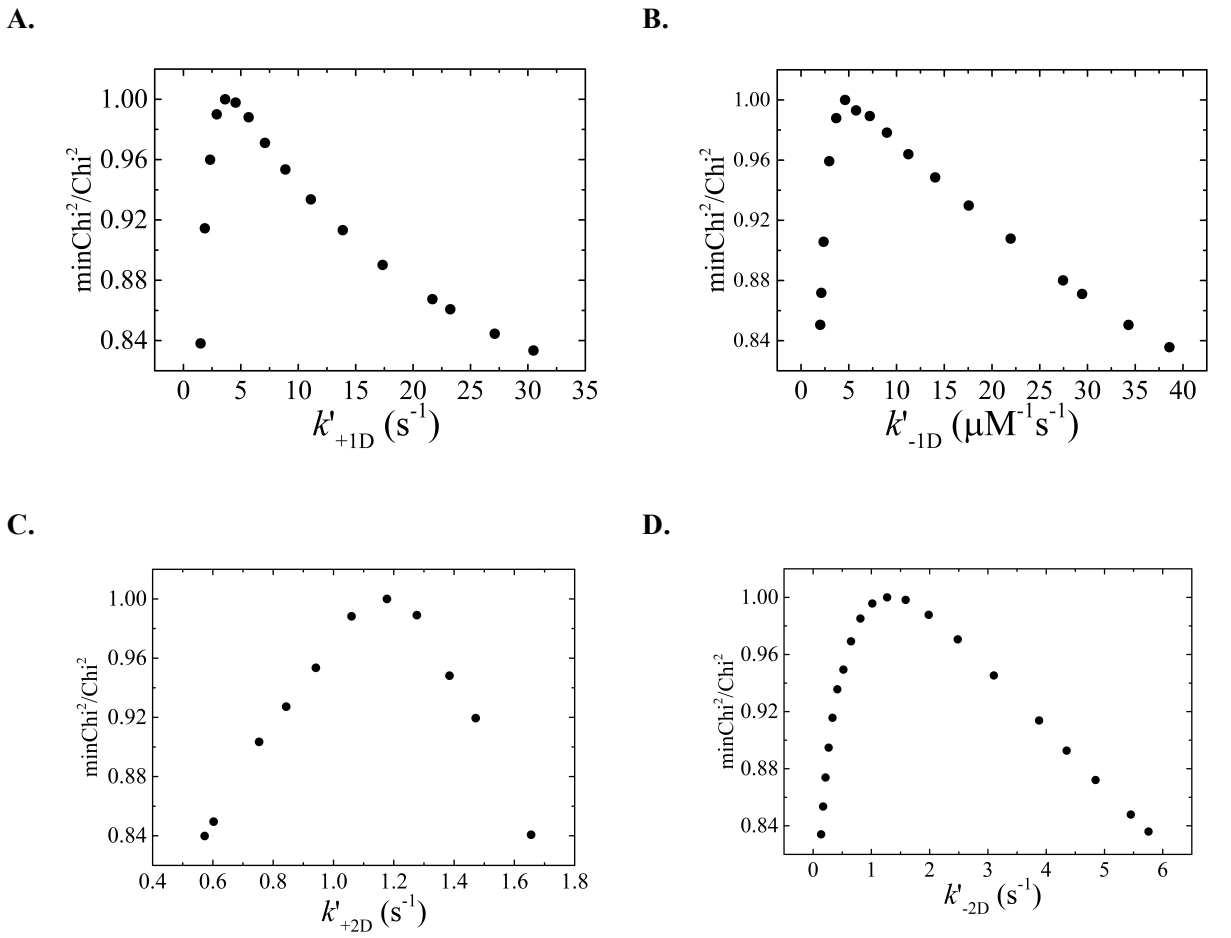

Figure S5. Goodness of the global fit parameters of ADP dissociation determined by ATP-induced dissociation of (pyrene)acto ·MYO1C

Chi^2 /$MinChi^2$ plots versus rate constants determined by global fit simulation for $MYO1C^C$. A threshold of 0.833 provides upper and lower limits, with best-fit values of **A.** k'_{+1D} = 3.6 ± 0.13 s^{-1}, **B.** k'_{-1D} = 4.6 ± 0.17 $\mu M^{-1} \cdot s^{-1}$, **C.** k'_{+2D} = 1.2 ± 0.01 s^{-1}, and **D.** k'_{-2D} = 1.3 ± 0.05 s^{-1} (Table 6). The simulations explore the range over which each parameter can vary while still allowing an acceptably good fit. While holding a given constant fixed, all other parameters were allowed to vary to seek the best fit to the data. The process is repeated over a range of parameter values to generate a plot of normalized chi^2 values (chi^2 divided by the minimum chi^2) versus the specific parameter value. All other constants in this simulation were fixed and determined by ATP-induced dissociation experiments together with the global fit simulation (Tables 3 and 4).

TABLES

Table S1: DNA oligos used for the generation of full length human MYO1C isoforms *constructs*

Construct	Primers (5'- 3')
*hs*MYO1C[35]	agcttgccctgggcagtgacggggttcgggtgaccATGGAGAGTGCGCTCACCGCC
	tccgcgtggttcatccccacaggccctgcaAGCTTGCCCTGGGCAGTGA
	atggcgctgcaagtggagctggtacccaccggggagatcaTCCGCGTGGTTCATCCCCA
*hs*MYO1C[16]	CGCGATCGCCATGGCGCTGCAAGTGGAGC
	CGCGATCGCCATGCGCTACCGGGCAT
*hs*MYO1C[C]	ATGGAGAGTGCGCTCACC
Universal C-terminal	CGTTTAAACCCGAGAATTCAGCCGTGGGGC

Table S2: Acto·MYO1C isoforms steady-state ATPase parameters

	MYO1C^{35}	MYO1C^{16}	MYO1C^{C}
K_{ATPase} (μM)	6.7 ± 1.57	10.6 ± 1.98	13.5 ± 2.00
k_{cat} (s^{-1}·$head^{-1}$)	0.09 ± 0.01	0.12 ± 0.01	0.09 ± 0.00

Conditions: 20 mM MOPS pH 7.0, 25 mM KAc, 2 mM $MgCl_2$, 0.2 mM EGTA, 1 mM DTT, 2 mM MgATP, 20 ± 0.1°C

Table S3: Acto·MYO1C binding affinities in the presence and absence of ADP

	MYO1C^{35}	MYO1C^{16}	MYO1C^{C}
K'_{A} (nM)	9.8 ± 2.41	65.8 ± 20.51	72.6 ± 17.94
Quenching %	25.6 ± 7.27	43.6 ± 4.67	65.1 ± 5.45
K'_{DA} (nM)[1]	12.3 ± 1.30	68.3 ± 36.24	83.1 ± 29.46
Quenching %	21.9 ± 0.49	44.7 ± 7.34	62.5 ± 7.27
K'_{DA}/K'_{A}*	1.40	0.99	1.39

Conditions: 20 mM MOPS pH 7.0, 25 mM KAc, 2 mM $MgCl_2$, 0.2 mM EGTA, 1 mM DTT, with 2 mM MgADP[1], 20 ± 0.1°C

* *Calculated*

Table S4: The amino acids sequences of the NTR peptides used for CD measurements

Peptide[1]	**Sequence (N terminal to C-terminal)**
NTR^{35}	MALQVELVPTGEIIRVVHPHRPCKLALGSDGVRVT
NTR^{35R21G}	MALQVELVPTGEIIRVVHPHGPCKLALGSDGVRVT
NTR^{16}	MRYRASALGSDGVRVT

[1]Peptides were resuspended in 20 mM MOPS pH 7.0, 25 mM KCl, heated for 30 min. at 50°C and slowly cooled to RT.

Table S5: Secondary structure prediction of the CD measurements presented at Figure 7 using the BestSel server (http://bestsel.elte.hu/)

Peptide[1]	Antiparallel (%)	Turn (%)	Others (%)	NRMSD
NTR^{35}	38.3	14.5	47.2	0.04597
$NTR^{35\text{-}R21G}$	41.5	14.3	44.2	0.04824
NTR^{16}	43.1	13.1	43.8	0.12247

[1]Data was collected at 20°C and in 20 mM MOPS pH 7.0, 25 mM KCl

References

1. Criddle, A. H., Geeves, M. A., and Jeffries, T. (1985) The use of actin labelled with N-(1-pyrenyl)iodoacetamide to study the interaction of actin with myosin subfragments and troponin/tropomyosin. *Biochem J* **232**, 343-349